

Relationships Between Elastic Anisotropy and Thermal Expansion in $A_2\text{Mo}_3\text{O}_{12}$ Materials

Electronic Supplementary Information

Carl P. Romao, S. P. Donegan, J. W. Zwanziger and Mary Anne White

Computational Methods

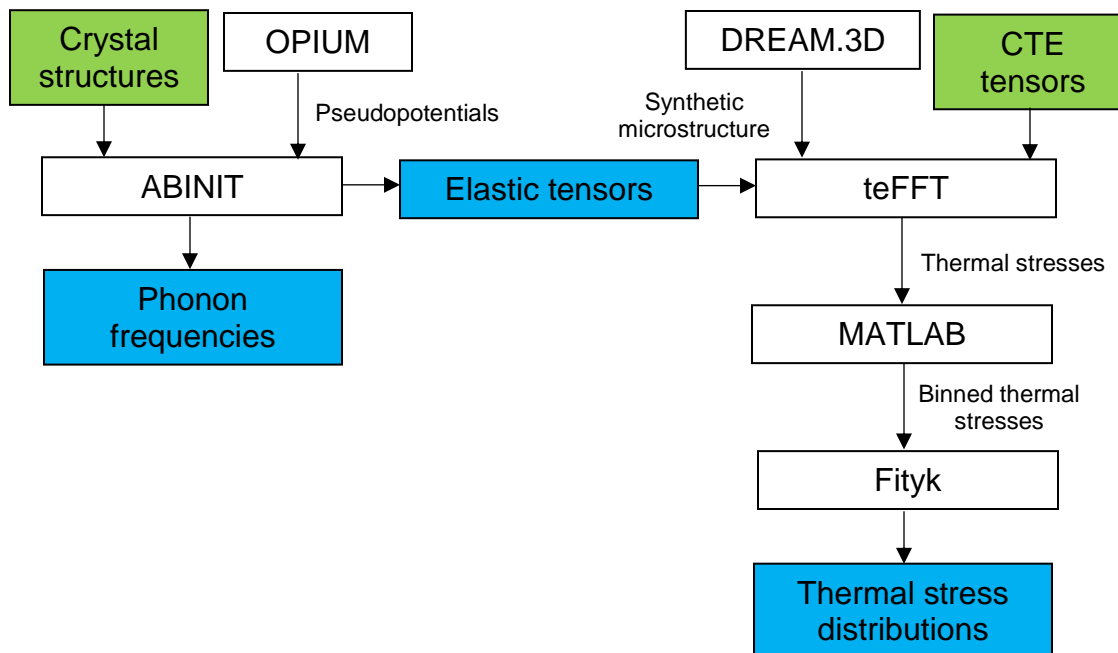


Figure S1: Flowchart showing the computational process used to generate the major results of this work. Green boxes indicate experimental data inputs, white boxes indicate software packages used herein, and blue boxes indicate results.

The spatially resolved thermal stress data were analysed following two separate local coordinate transformations performed using MATLAB:¹ one to the principal stresses (σ_1 , σ_2 , and σ_3) and one to the unit cell axes (σ_{aa} , σ_{bb} , σ_{cc} , σ_{bc} , σ_{ac} , and σ_{ab}). Statistical analysis of the resulting distributions using univariate distribution functions was subsequently attempted using R.² Several functions (normal, Cauchy, and logistic distributions) were trialed. The normal and logistic distributions showed reasonable fits to the data near the mean, but poorly predicted the extremal stresses. This method of fitting the data directly was limited by two factors: the large size of the data set and that the distribution function used must be able to handle negative and positive inputs (which excludes, for example, the Rayleigh, gamma, two-parameter Weibull, and

¹ MATLAB – Mathworks, <http://www.mathworks.com/products/matlab> (accessed 02/05/16).

² R: The R Project for Statistical Computing, <http://www.r-project.org> (accessed 02/05/16).

two-parameter lognormal distributions). To avoid these limitations a different method was adopted.

Using MATLAB, the thermal stress data points were sorted into histograms, with 500 kPa bin sizes. This binning allowed more functions and combinations of functions to be trialed because of the large reduction in the size of the data set to be analysed, at the expense of some added granularity. The use of histograms shifts the problem from a univariate fitting of statistical distributions to a two-dimensional problem of finding functions that fit the histograms to approximate the underlying distributions. Due to the large starting data set, the bin sizes could be made very small and the resulting histograms are accurate representations of the thermal stress distributions. Curve-fitting was carried out using the program Fityk.^{3,4}

No single function was found to fit the stress distributions in the eigenbasis or the unit cell axis basis. Instead, multiple curves were required. In all cases, the uniaxial stress distributions showed significant skewing and shoulders were visible in the shear stress distributions (particularly σ_{ac} and σ_{ab}). The four-parameter lognormal distribution⁵ was determined to provide satisfactory fits to the stress distributions in the eigenbasis and the unit cell basis using only two curves (see below), while the normal distribution required three to avoid underestimation of the extremal stresses. The use of two curves is more justifiable than three since thermal stress is caused by interactions of one axis with the thermal expansion of the other two.

Stresses in previously reported finite-element analyses⁶ were considerably higher than the previous results, with maxima greater than 2 GPa. The differences can be attributed to the differences in the modeled microstructures. The finite-element model was limited by computational constraints to cubic crystallites, which led to larger stresses since as many as eight misaligned grains could meet at a vertex. This effect is evidently greater than the stress decrease caused by the small size and unrestrained boundary conditions used in the finite-element model of $\text{Y}_2\text{Mo}_3\text{O}_{12}$. The current model uses a more realistic microstructure which entails fewer grains meeting at each grain edge and boundary, and subsequently less thermal expansion mismatch on average per grain. Unlike models from previous studies,^{6,7} the number of grains in the simulated microstructure should be large enough that the surface effects on the average strain energy density are minimal. The difference can now be attributed to elastic anisotropy, as discussed in the main text.

³ M. J. Wojdyr, *Appl. Cryst.*, 2010, **43**, 1126–1128.

⁴ Fityk – curve fitting and peak fitting software, <http://fityk.nieto.pl> (accessed 02/05/16) .

⁵ D. B. Siano and D. E. Metzler, *J. Chem. Phys.*, 1969, **51**, 1856–1861.

⁶ C. P. Romao, K. J. Miller, M. B. Johnson, J. W. Zwanziger, B. A. Marinkovic, and M. A. White, *Phys. Rev. B*, 2014, **90**, 024305.

⁷ L. P. Prisco, C. P. Romao, M. A. White, and B. A. Marinkovic, *J. Mater. Sci.*, 2013, **48**, 2986–2996.

Phonon Frequencies

Table S1: Calculated Γ -point vibrational frequencies of $\text{Al}_2\text{Mo}_3\text{O}_{12}$ from ABINIT.

ν / cm^{-1}										
25.96	110.11	170.52	234.35	287.27	331.63	373.06	441.15	843.82	946.97	
55.52	114.64	171.16	235.35	287.89	334.86	381.19	443.73	846.83	948.57	
61.39	115.71	174.70	248.59	290.30	338.57	383.41	445.56	848.33	950.10	
65.54	119.44	175.18	249.40	292.83	339.14	395.08	462.33	849.18	950.83	
72.13	125.94	180.97	252.03	298.91	339.30	398.72	475.26	850.55	965.11	
74.17	127.97	188.63	259.95	299.21	342.26	402.66	477.97	850.57	968.23	
75.87	130.31	195.48	260.80	300.20	342.88	403.34	782.36	852.98	970.29	
78.15	134.98	197.60	261.84	302.37	343.68	404.96	783.82	853.17	977.53	
78.19	135.62	199.00	264.77	303.97	346.93	405.78	785.27	853.86	979.73	
80.89	142.03	199.02	265.45	304.97	347.10	406.79	787.34	856.40	981.60	
84.19	142.27	200.12	269.32	306.72	349.03	407.60	787.89	860.59	984.13	
85.63	143.97	209.23	270.78	307.60	352.32	408.44	790.89	861.10	985.50	
89.13	147.95	209.74	271.28	312.55	360.82	408.58	793.92	862.96		
89.35	148.08	214.27	273.26	315.43	361.12	408.58	796.97	863.96		
91.98	148.54	218.39	273.57	319.35	361.58	412.42	799.76	922.02		
95.87	151.00	218.98	277.29	319.78	366.21	420.82	801.17	922.91		
100.36	153.81	219.88	278.09	321.99	366.93	425.19	810.93	929.65		
103.50	154.25	223.85	283.50	322.66	367.84	426.27	832.54	932.28		
106.12	160.49	225.74	286.30	326.71	368.06	434.33	836.55	934.50		
106.32	163.32	225.92	286.45	328.14	368.26	434.41	840.12	943.18		
106.69	170.50	233.39	286.70	328.46	372.98	437.26	842.50	944.95		

Table S2: Calculated Γ -point vibrational frequencies of $\text{ZrMgMo}_3\text{O}_{12}$ from ABINIT. ν / cm^{-1}

43.18	88.24	135.13	199.01	262.55	298.59	327.30	371.65	815.60	955.54
46.47	89.32	136.47	200.63	266.27	300.50	330.50	371.67	821.76	955.61
46.84	89.64	141.49	208.19	268.75	301.44	333.12	372.41	824.53	956.05
48.13	92.01	141.90	214.36	271.65	303.95	334.47	378.56	825.06	957.03
54.67	92.80	143.36	214.84	273.90	309.75	336.21	380.25	832.72	960.60
55.24	95.87	145.85	216.11	274.83	311.18	338.08	386.19	871.21	966.06
56.24	101.18	146.33	221.48	275.85	312.28	338.68	717.69	871.85	968.55
57.74	101.41	156.17	222.15	279.45	312.65	340.60	719.29	873.79	969.09
57.96	102.58	158.04	223.06	279.88	313.37	340.90	719.50	899.93	970.50
66.48	103.15	160.28	224.46	280.43	313.74	340.91	722.45	901.28	980.58
66.57	107.93	162.16	228.48	283.80	316.37	346.26	723.96	901.89	980.80
66.77	108.47	165.50	233.86	284.79	317.01	346.50	724.20	903.15	983.22
71.19	110.36	171.38	234.75	286.94	318.90	346.55	733.11	904.77	
76.11	110.44	173.51	240.09	288.73	319.41	351.37	734.30	905.41	
76.56	111.61	173.74	244.72	289.87	320.30	352.39	735.08	939.41	
78.19	118.33	174.29	245.97	291.10	320.54	352.68	788.97	941.50	
78.72	119.60	178.58	249.63	292.03	321.13	356.54	792.89	948.20	
78.74	125.08	179.10	251.51	294.20	324.03	356.90	793.88	949.22	
83.03	126.36	182.32	261.60	294.36	324.23	363.55	798.10	949.41	
84.38	127.12	183.29	262.08	295.07	326.37	363.93	803.49	953.92	
87.26	129.18	186.43	262.35	297.28	326.47	364.59	814.97	955.07	

Table S3: Calculated Γ -point vibrational frequencies of $\text{Sc}_2\text{Mo}_3\text{O}_{12}$ from ABINIT. ν / cm^{-1}

21.11	85.72	124.79	185.07	244.21	280.04	349.56	426.46	894.35	994.62
22.51	85.98	126.00	187.69	245.69	281.49	352.80	431.13	904.87	994.99
29.17	87.20	131.82	192.75	245.98	285.84	357.86	451.05	909.10	998.10
36.08	89.65	133.93	196.71	250.67	288.98	361.79	461.32	909.30	998.17
38.08	91.21	135.54	198.74	250.87	293.07	363.04	462.26	909.72	1009.41
42.77	91.78	136.71	201.31	252.54	293.59	367.22	462.44	928.91	1016.12
48.66	93.06	141.09	214.02	254.71	294.27	374.23	812.68	929.57	1023.06
50.04	96.62	142.12	218.01	254.87	294.80	390.93	813.83	935.61	1026.19
52.77	96.98	145.43	218.38	256.20	301.93	391.17	816.34	951.45	1027.11
53.87	98.38	152.10	219.61	257.70	302.19	393.24	817.64	952.06	1031.22
55.17	98.46	152.87	222.43	259.11	308.46	393.45	823.75	952.47	1031.75
57.28	101.13	157.98	223.97	260.80	313.40	398.34	824.52	957.75	1033.45
63.20	104.38	161.67	225.03	262.06	319.62	400.21	841.86	963.95	
63.63	106.09	163.87	227.36	265.03	321.25	402.92	845.09	966.59	
67.81	109.44	164.41	227.81	266.65	323.86	403.75	847.13	978.80	
72.42	113.19	166.88	230.26	267.62	324.36	419.38	871.47	988.59	
76.20	113.51	178.92	230.73	270.74	327.31	419.49	873.03	989.59	
78.10	115.88	179.36	235.77	271.60	335.10	420.41	882.56	991.17	
78.48	117.41	182.47	239.18	274.03	335.24	420.69	884.06	992.47	
81.14	119.01	182.74	240.82	278.31	337.62	424.69	889.14	993.05	
85.71	120.17	184.46	241.16	279.50	348.75	425.71	891.22	994.54	

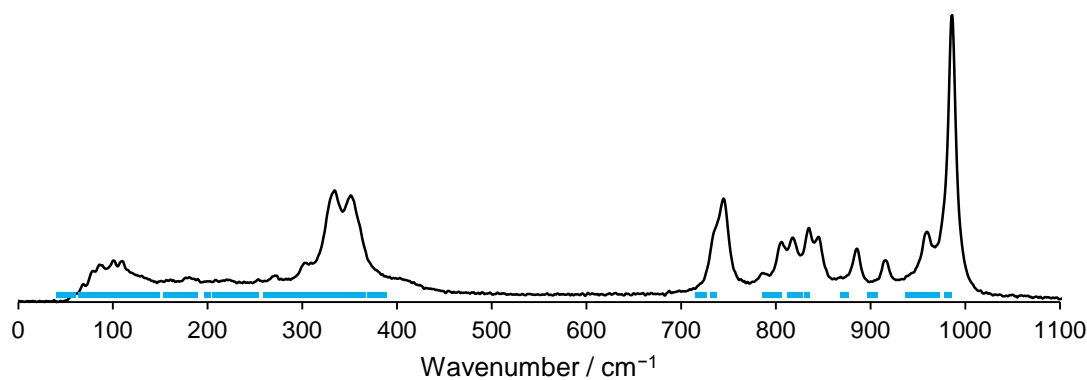
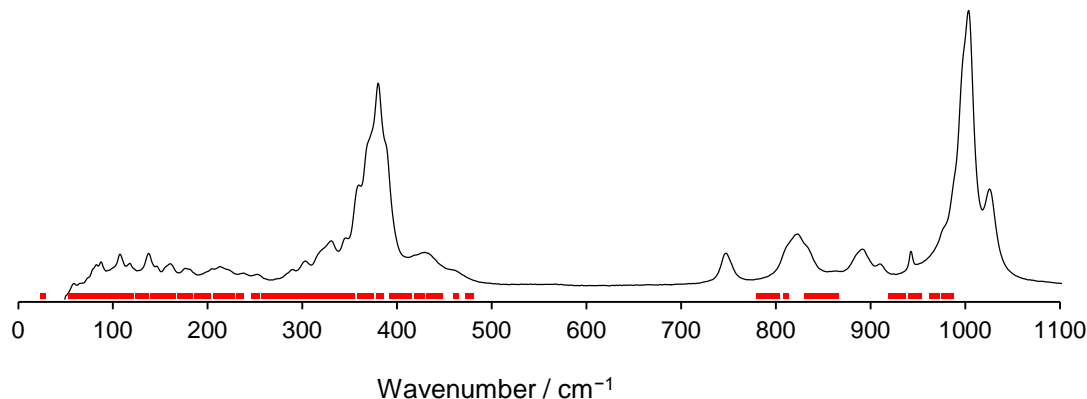


Figure S2: Experimental Raman spectra^{8,9} (black line) compared to calculated Γ -point optic phonon frequencies of $\text{Al}_2\text{Mo}_3\text{O}_{12}$ and $\text{ZrMgMo}_3\text{O}_{12}$.

⁸ L. P. Prisco, P. I. Ponton, W. Paraguassu, C. P. Romao, M. A. White, and B. A. Marinkovic, “Near-zero thermal expansion and phase transition in $\text{In}_{0.5}(\text{ZrMg})_{0.75}\text{Mo}_3\text{O}_{12}$,” in press in *J. Mater. Res.*.

⁹ C. P. Romao, F. A. Perras, U. Werner-Zwanziger, J. A. Lussier, K. J. Miller, C. M. Calahoo, J. W. Zwanziger, M. Bieringer, B. A. Marinkovic, D. L. Bryce, and M. A. White, *Chem. Mater.*, 2015, **27**, 2633–26476.

Thermal Stress Distributions

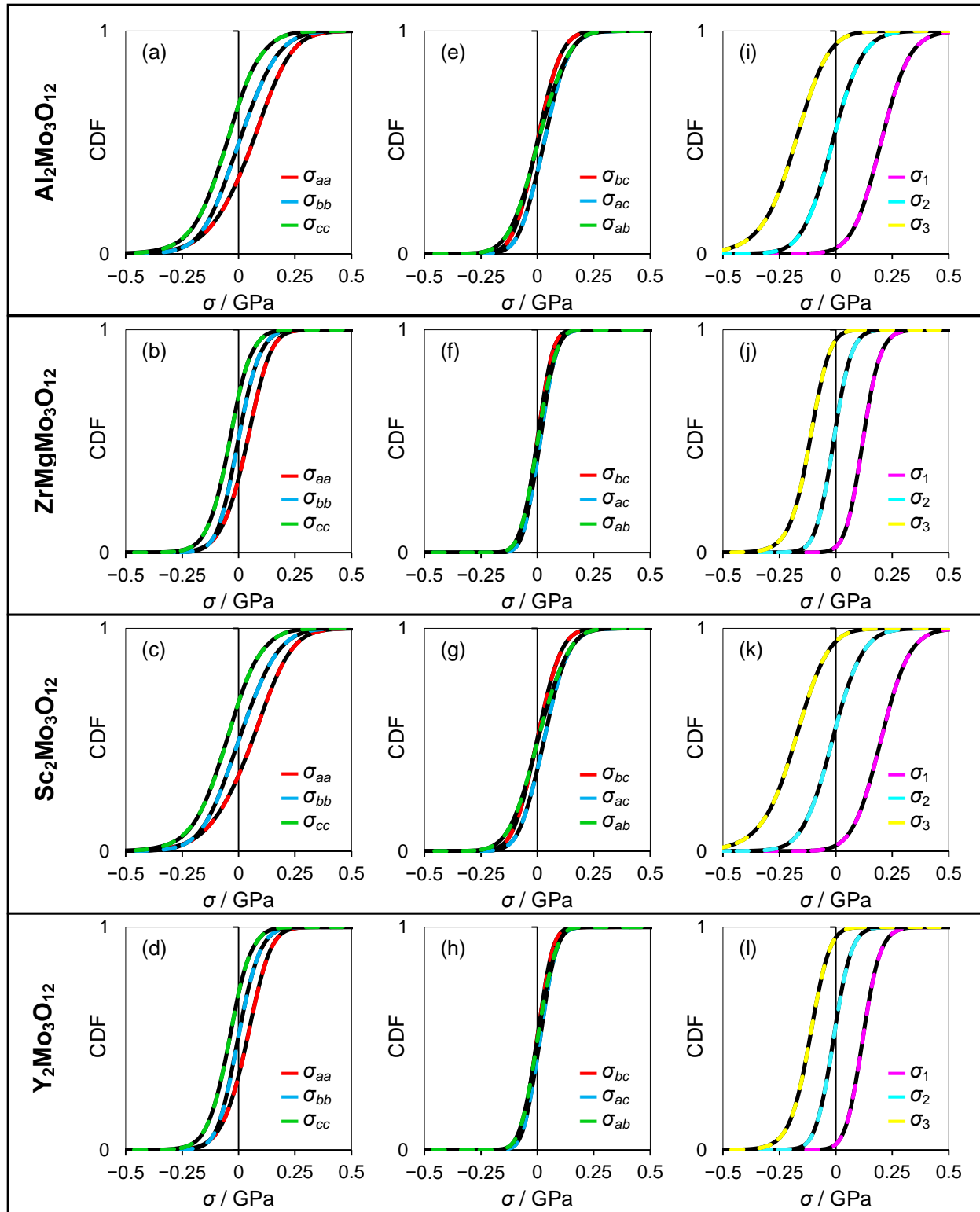


Figure S3: Cumulative distribution functions of thermal stress in $\text{Al}_2\text{W}_3\text{O}_{12}$, $\text{ZrMgMo}_3\text{O}_{12}$, $\text{Sc}_2\text{Mo}_3\text{O}_{12}$ and $\text{Y}_2\text{Mo}_3\text{O}_{12}$ in (a)–(h) the unit cell basis, and (i)–(l) the eigenbasis. Solid black lines are data, dashed coloured lines are fits to the data.

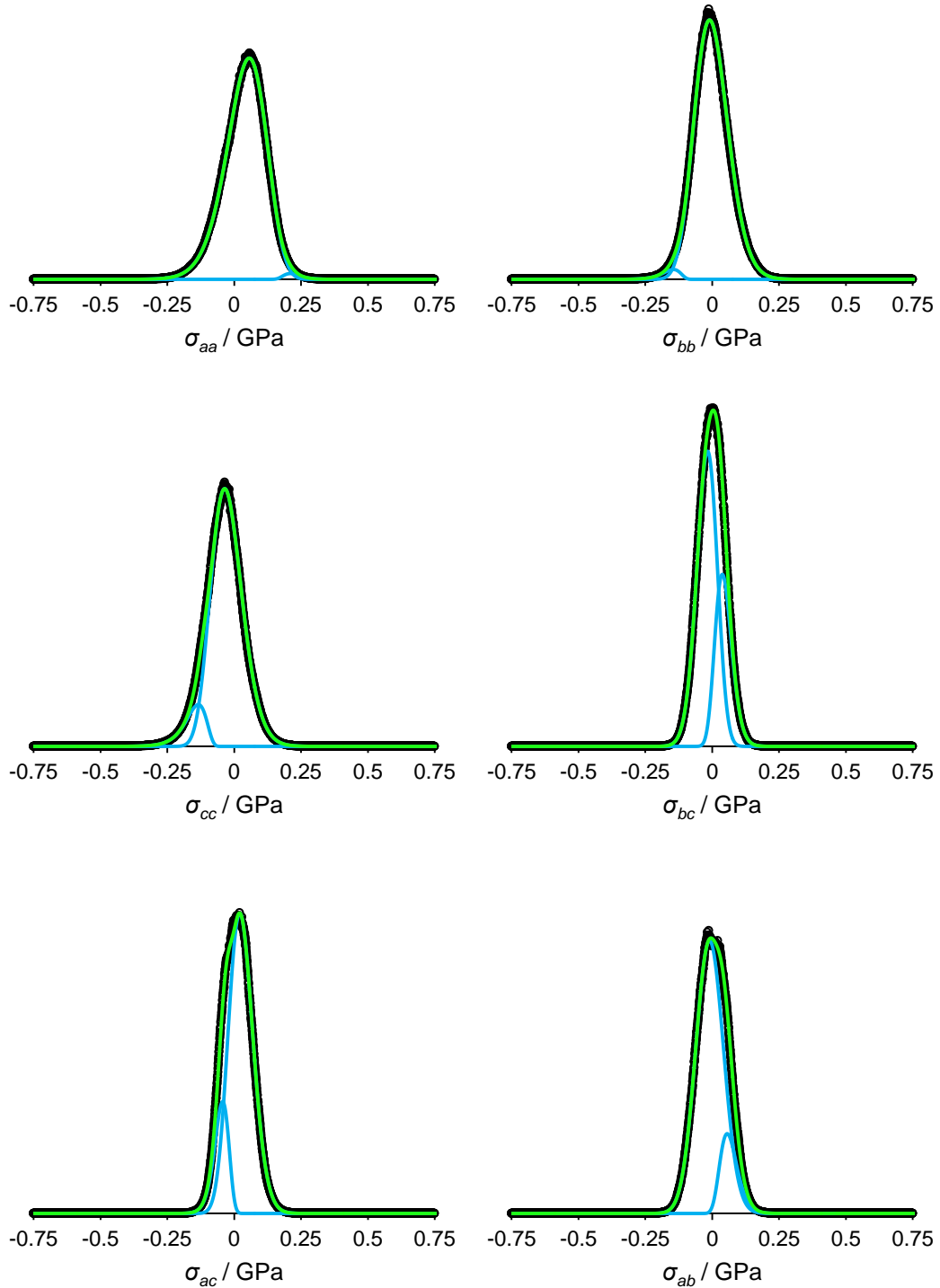


Figure S4: PDFs of thermal stress in the unit cell basis for polycrystalline $\text{Al}_2\text{Mo}_3\text{O}_{12}$ following cooling by 700 K. Black points are data, green lines are the fit to the data, and blue lines are the lognormal functions which compose the fit.

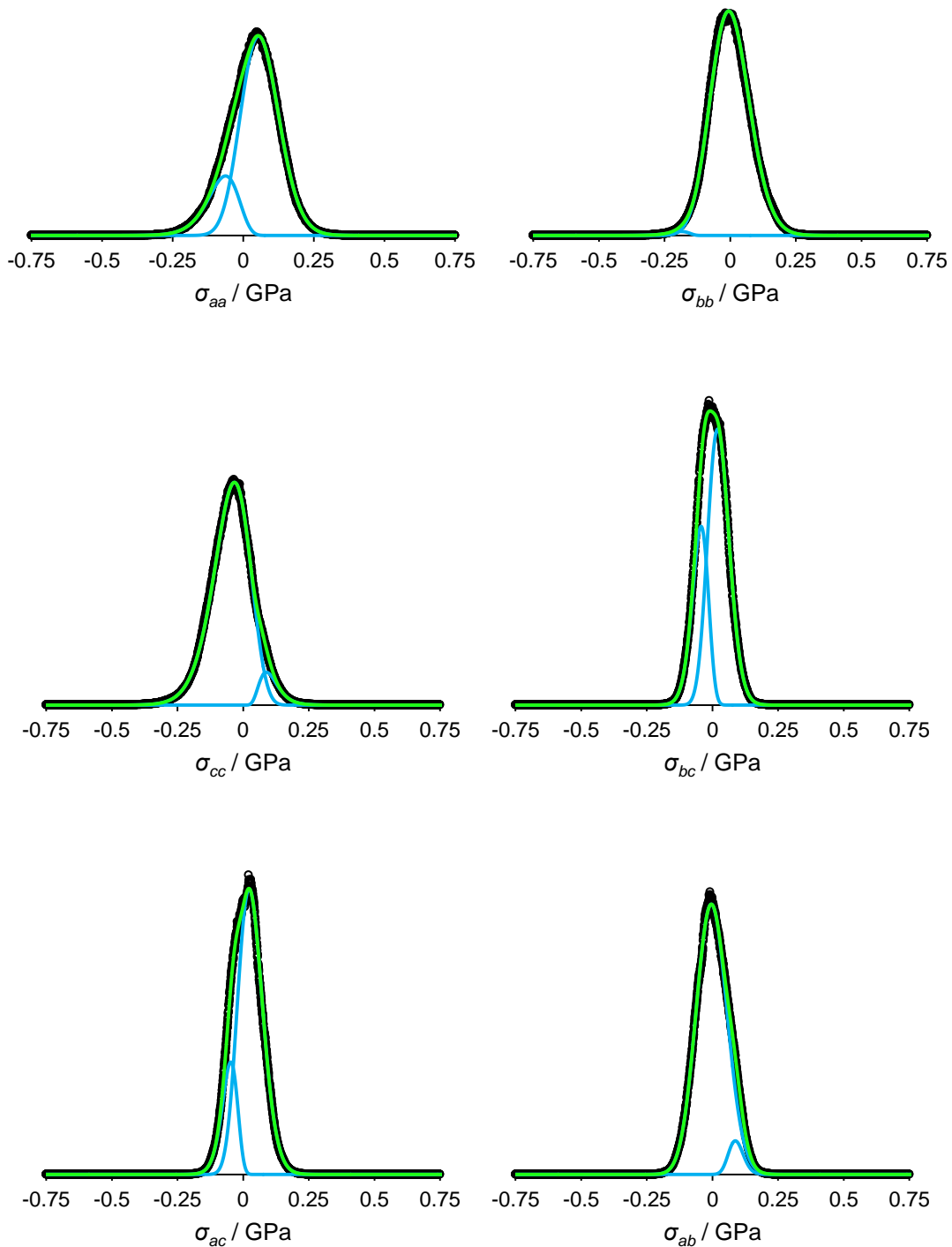


Figure S5: PDFs of thermal stress in the unit cell basis for polycrystalline $\text{ZrMgMo}_3\text{O}_{12}$ following cooling by 700 K. Black points are data, green lines are the fit to the data, and blue lines are the lognormal functions which compose the fit.

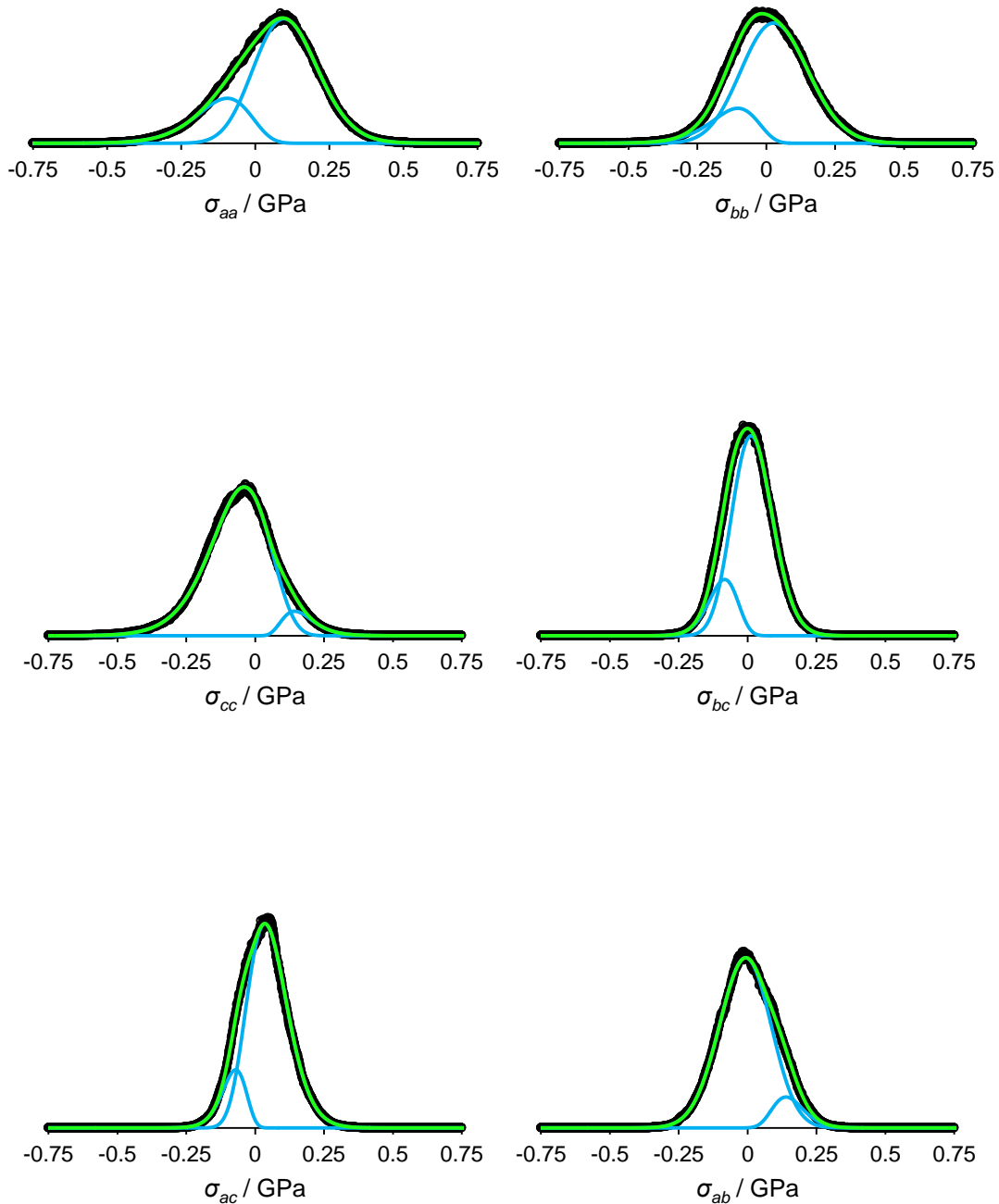


Figure S6: PDFs of thermal stress in the unit cell basis for polycrystalline $\text{Sc}_2\text{Mo}_3\text{O}_{12}$ following cooling by 700 K. Black points are data, green lines are the fit to the data, and blue lines are the lognormal functions which compose the fit.

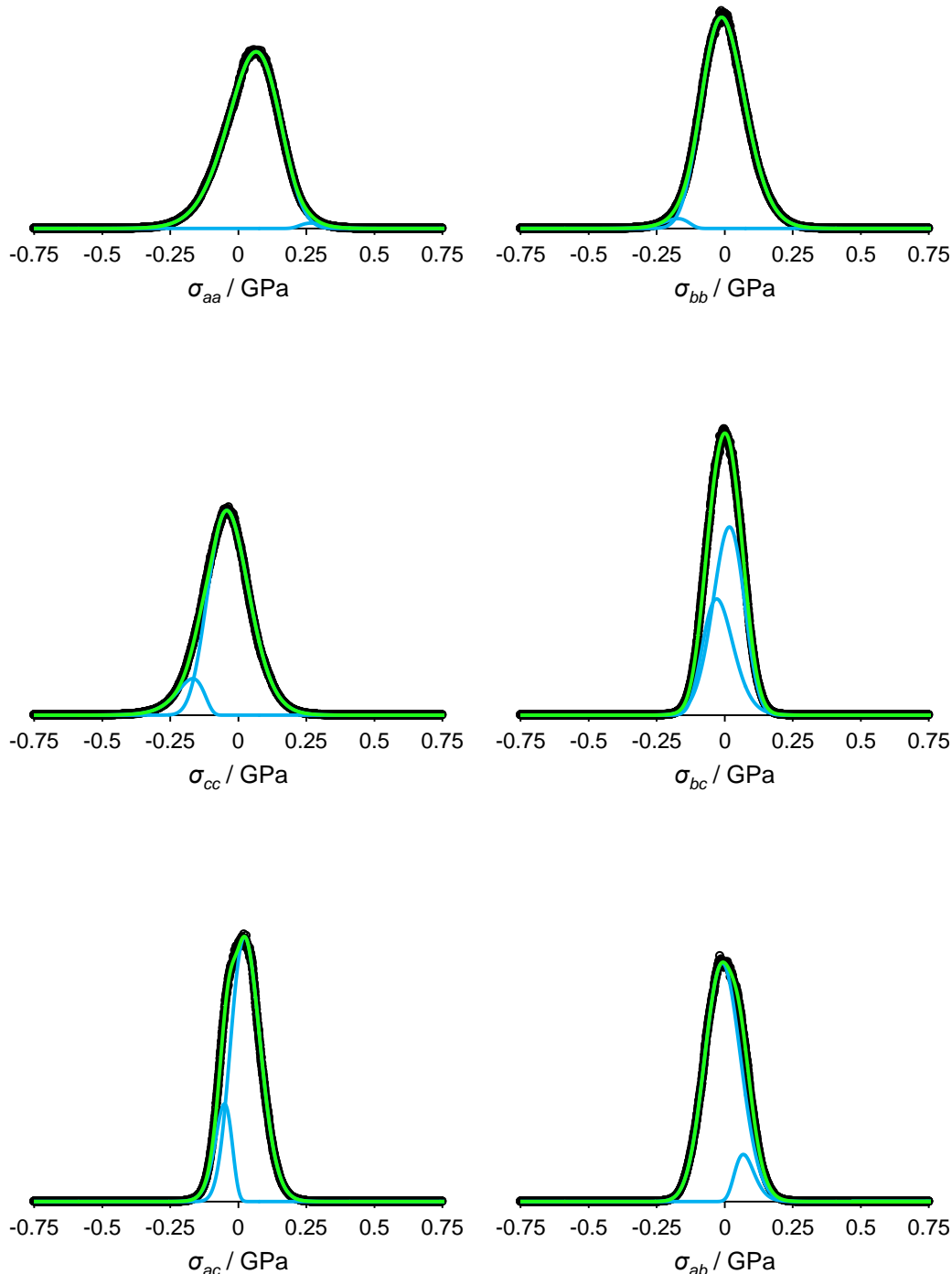


Figure S7: PDFs of thermal stress in the unit cell basis for polycrystalline $\text{Y}_2\text{Mo}_3\text{O}_{12}$ following cooling by 700 K. Black points are data, green lines are the fit to the data, and blue lines are the lognormal functions which compose the fit.

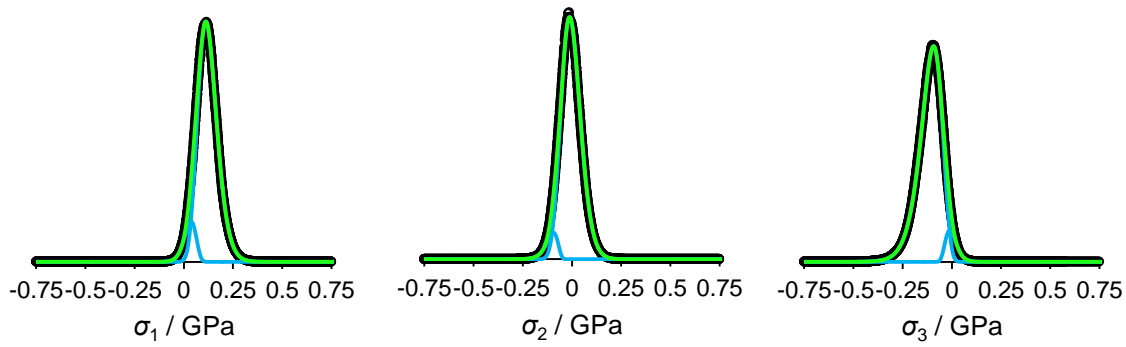


Figure S8: PDFs of thermal stress in the eigenbasis for polycrystalline $\text{Al}_2\text{Mo}_3\text{O}_{12}$ following cooling by 700 K. Black points are data, green lines are the fit to the data, and blue lines are the lognormal functions which compose the fit.

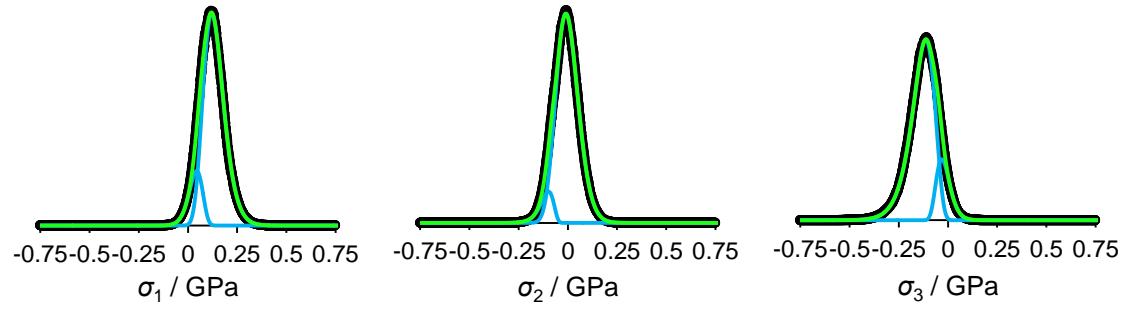


Figure S9: PDFs of thermal stress in the eigenbasis for polycrystalline $\text{ZrMgMo}_3\text{O}_{12}$ following cooling by 700 K. Black points are data, green lines are the fit to the data, and blue lines are the lognormal functions which compose the fit.

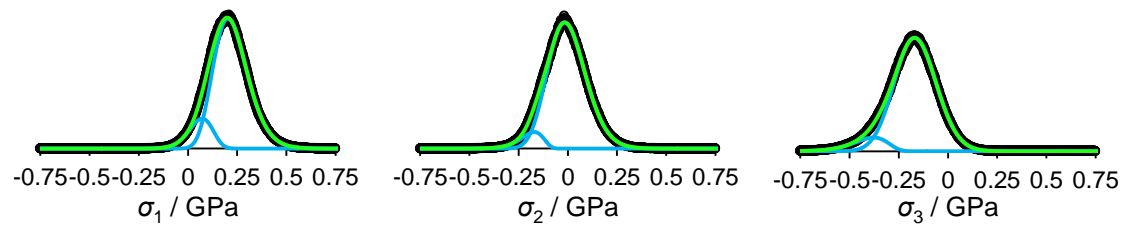


Figure S10: PDFs of thermal stress in the eigenbasis for polycrystalline $\text{Sc}_2\text{Mo}_3\text{O}_{12}$ following cooling by 700 K. Black points are data, green lines are the fit to the data, and blue lines are the lognormal functions which compose the fit.

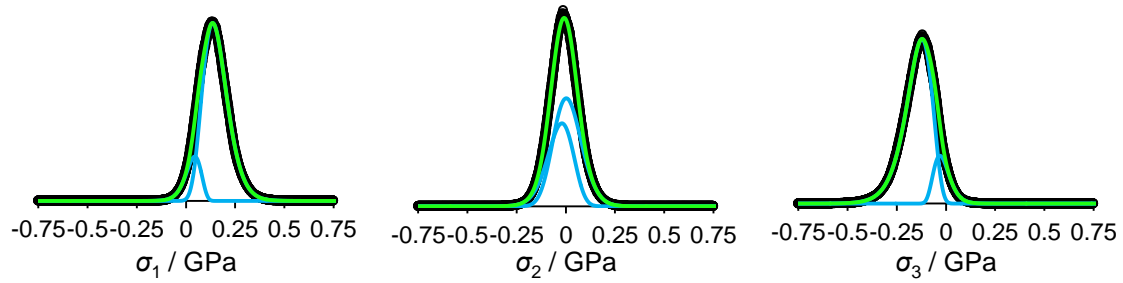


Figure S11: PDFs of thermal stress in the eigenbasis for polycrystalline $\text{Y}_2\text{Mo}_3\text{O}_{12}$ following cooling by 700 K. Black points are data, green lines are the fit to the data, and blue lines are the lognormal functions which compose the fit.